JOURNAL OF MATERIALS SCIENCE **38** (2003) 3783–3790

Effect of surfactant concentration and composition on the structure and properties of sol-gel-derived bioactive glass foam scaffolds for tissue engineering

J. R. JONES, L. L. HENCH
Department of Materials, Imperial College London, South Kensington Campus, London SW7 2BP, UK
E-mail: julian.r.jones@imperial.ac.uk

Bioactive glasses are known to have the ability to regenerate bone, and to release ionic biological stimuli that promote bone cell proliferation by gene activation, but their use has been restricted mainly to the form of powder, granules or small monoliths. Resorbable 3D macroporous bioactive scaffolds have been produced for tissue engineering applications by foaming sol-gel-derived bioactive glasses. The foams exhibit a hierarchical structure, with interconnected macropores (10–500 μm), which provide the potential for tissue ingrowth and mesopores (2–50 nm), which enhance bioactivity and release of ionic products. The macroporous matrices were produced by the foaming of sol-gel glasses with the use of a surfactant. Three glass systems SiO_2, SiO_2-CaO and SiO_2-CaO-P_2O_5 were foamed using various concentrations of surfactant, in order to investigate the effect of surfactant concentration and composition on the structure and properties of the hierarchical construct.

1. Introduction

Harvesting a patient's tissue from a donor site and transplanting it to a host site while maintaining blood supply is the gold standard for the repair of bone defects (autografts). Autografts and homografts (where tissue is harvested from another patient) have the important limitations of low availability and second site morbidity. Homografts also require the use of immunosuppresant drugs. As life expectancy increases, a shift in emphasis is required from the replacement of tissues and donors to the fields of tissue engineering and tissue regeneration, which aim to restore diseased and damaged tissues to their natural form [1].

Tissue regeneration techniques involve the use of a scaffold that can be implanted into a defect to regenerate a tissue *in situ*. In tissue engineering applications the scaffolds are seeded with cells *in vitro* to produce the basis of a tissue before implantation [2].

Certain compositions of melt-derived bioactive glasses containing SiO_2-CaO-P_2O_5 bond to both soft and hard tissue *in vivo* without forming scar tissue [3]. The bioactivity has been associated with the formation of a crystalline hydroxycarbonate apatite (HCA) surface layer, which has a similar structure to that of bone mineral, on contact with body fluid [4]. Recently, Xynos *et al.* [5] have shown that bioactive glass dissolution products cause rapid expression of genes that regulate osteogenesis and the production of growth factors. These discoveries have stimulated extensive investigations for using bioactive glass as scaffolds for tissue engineering.

An ideal scaffold should combine these properties with a structure consisting of an interconnected macroporous network (with pore diameters in excess of 100 μm) to enable tissue ingrowth [6] and nutrient delivery to the centre of the regenerated tissue and a surface texture that promotes cell adhesion. The scaffold should be resorbable at controllable rates and be made from a processing technique that can produce irregular shapes to match that of the defect in the bone of the patient.

The foaming of sol-gel derived bioactive glasses provides the potential to make such a scaffold [7]. Sol-gel derived glasses exhibit enhanced bioactivity and resorbability compared to melt-derived glasses of similar composition [8–10] due to the presence of a mesoporous texture (pores with diameters in the range 2 nm–50 nm), which is inherent to the sol-gel process. The mesoporous texture causes the gel-glasses to have a high specific surface area and provides nucleation sites for the HCA layer [11].

Many factors in the process affect the structure and properties of the foam scaffolds and can be used to obtain specific architectures, to produce specific pore size ranges and controlled rates of glass dissolution. These variables must be fully investigated if the properties of the foam scaffolds are to optimised. This work concentrates on the effect of surfactant concentration

and composition on the structure and properties of the scaffold.

2. Experimental

2.1. Sol preparation

The sol-gel preparation was carried out using three glass compositions: pure silica SiO_2 (100S), the binary 70 mol% SiO_2-30 mol% CaO (70S30C), and the ternary 60 mol% SiO_2, 36 mol% CaO, 4 mol% P_2O_5 (58S) systems. Sol-gel precursors used were tetraethoxyl orthosilicate (TEOS, $Si(OC_2H_5)_4$), triethoxyl orthophosphate (TEP, $OP(OC_2H_5)_3$), and calcium nitrate $Ca(NO_3)_2{\cdot}4H_2O$, for 58S [9]; TEOS and $Ca(NO_3)_2{\cdot}4H_2O$ only were used for 70S30C and TEOS only for 100S [12].

2.2. Foaming

Simultaneous hydrolysis and polycondensation reactions occur during and after sol preparation, forming the basis of a silica network.

On completion of hydrolysis, aliquots of 50 ml of sol were foamed by vigorous agitation at 25°C (in a thermostatically controlled water bath) with the addition of 0.25, 0.5, 0.65, 0.75, 1.0, 1.25, 1.5, 2.0, or 3 ml of surfactant. The surfactant used was Teepol (Thames Mead Ltd.), a general-purpose detergent containing a low concentration (less than 3 vol%) mixture of anionic and nonionic surfactants. The surfactant stabilises the bubbles that are formed by air entrapment during the early stages of foaming by lowering the surface tension of the solution. The concentration of surfactant was varied to obtain specimens of various fractions of porosity. The polycondensation reaction (gelation) was catalysed with addition of 1.5 ml HF. As viscosity rapidly increased and the gelling point was approached the solution was cast into airtight moulds. The gelation process provides permanent stabilisation for the bubbles. The samples were then aged at 60°C for 72 h, dried at 130°C for 48 h and thermally stabilised at 600°C for 22 h, according to established procedures [12]. At least three separate batches were produced for each surfactant concentration and each composition to ensure reproducibility.

Sol-gel derived bioactive glass monoliths of the three compositions were also produced, in the unfoamed state, but with equivalent concentrations of surfactant and HF as the foam samples.

2.3. Characterisation

The resulting foams and monoliths were characterised using a field emission scanning electron microscopy (Leo 1525) with 2 kV accelerating voltage, mercury porosimetry (PoreMaster 33, Quantachrome) and nitrogen adsorption (Autosorb AS6, QuantaChrome) to measure macropore [13] and mesopore [14] size distributions respectively. B.E.T. analysis was used to determine the specific surface area [14]. The pore diameter distribution was calculated by the BJH method applied to the N_2 desorption curves [14]. The types of isotherms were evaluated according to their shape and type of hysteresis between adsorption-desorption modes. Skeletal and bulk densities were measured by helium pycnometry and geometrical methods respectively.

Differential thermal analysis (DTA) and thermal gravimetric analysis (TGA) were carried out on dried (unstabilised) foams and monoliths of 58S and 70S30C compositions in order to monitor the effect of composition, surfactant concentration and porosity on the crystallisation point of gel-glasses. Platinum crucibles containing 35 mg of sample were heated in air at a rate of 10°C min^{-1} to 1200°C using a Stanton Redcroft STA-780 series thermal analyser with Al_2O_3 as the reference material.

3. Results

3.1. Observations during processing

Fig. 1 shows a graph of foam volume as a function of surfactant concentration for each of the three bioactive glass compositions. The foam volume is the first indication of how porous a foamed scaffold will be as the larger the foam volume the larger will be the mean pore size. Fig. 1 shows that the binary 70S30C glass was the most susceptible to foaming, producing a maximum of 300 ml foam from 50 ml sol (a 6-fold increase). Foam volumes greater than 225 ml (foam survival limit, Fig. 1) were unstable as pores became so large and the pore walls so thin that they could not support the weight of the foam. The foam survival limit was dependent on the strength of the liquid pore walls prior to gelling [15], which primarily depends on the foam volume. The maximum foam volume is associated with a critical thickness of the pore wall liquid film that can support the weight of the foam. The thickness of the liquid film decreased as foam volume and bubble diameter increased. The other gel compositions did not reach their survival limits no matter how much surfactant was added. Added water is needed for these compositions to produce large foam volumes. The tertiary 58S system was the least susceptible to foaming, producing a maximum foam volume of 107 ml from 50 ml of sol (a 2-fold increase). The unary 100S exhibited a slightly greater foamability than the 58S system.

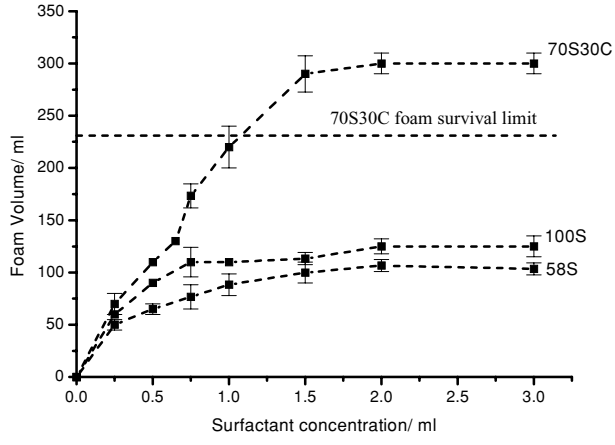

Figure 1 Graph of foam volume attained after vigorous agitation, as a function of surfactant concentration, for three glass compositions.

TABLE I Summary of the characterisation of scaffolds foamed at different concentrations of Teepol. Surface area, mesopore volume, mesopore diameter and pore volume were determined by nitrogen adsorption. Modal macropore diameter was determined using mercury intrusion porosimetry

Glass	Teepol conc. (ml)	Foam volume (ml)	Bulk density (gcm^{-3})	Surface area (m^2g^{-1})	Modal mesopore size (nm)	Modal macropore size (μm)
58S	0	0	0.86	155.6	9.5	0
	0.50	65	0.60	153.4	9.6	0
	0.75	77	0.48	182.3	9.5	7.0
	1.0	88	0.36	201.7	9.6	18.5
	1.5	100	0.39	220.1	9.7	19.9
	2.0	106	0.35	170.0	12.4	20.3
	3.0	104	0.41	175.1	12.2	33.6
70S30C	0	0	0.71	134.7	17.4	0
	0.25	80	0.33	134.7	17.5	6.0
	0.50	110	0.25	137.2	17.6	91.0
	0.65	130	0.18	125.5	29.4	82.0
	0.75	180	0.15	150.3	17.6	139.0
	1.0	200	0.15	144.1	17.5	132.0
SiO_2	0	0	0.98	646.0	3.8	0
	0.50	90	0.27	282.7	17.1	41.3
	0.75	110	0.18	301.6	12.1	44.0
	1.0	110	0.24	293.6	17.2	71.0
	1.5	113	0.22	278.5	17.0	53.7
	2.0	125	0.17	287.3	17.5	30.9
	3.0	125	0.16	276.7	17.4	64.9

Fig. 1 shows that the foam volume achieved from 50 ml of initial sol increased as surfactant concentration increased until a point where the sol became saturated with surfactant. The saturation point for each composition was at approximately 1.5 ml of added surfactant, however the foam volume was much higher (230 ml) for the 70S30C composition compared to 110 ml and 100 ml exhibited by 100S and 58S foams respectively.

Table I summarises the properties of the foam scaffolds produced in this study. All values are mean values from $n > 3$. The table is in three main sections; one for each glass composition. Different values of surfactant concentration were used for each glass composition due to the different foamability of each glass system.

Table I shows that as the foam volume increased (i.e., surfactant concentration increased) the bulk density (ρ_b) of all the foams generally decreased. The 70S30C composition exhibited the greatest change in ρ_b, unfoamed monoliths had a ρ_b of 0.71 gcm^{-3} whereas ρ_b was 0.15 gcm^{-3} when the sol was foamed with 0.75 ml surfactant. The minimum ρ_b of 58S foam was 0.35 gcm^{-3}, which was produced using 2 ml surfactant.

3.2. Macropore characterisation

The architecture of the two elements of the hierarchical structure (the interconnected macroporous network and mesoporous texture) will now be discussed.

3.2.1. 58S foams

Fig. 2 shows SEM micrographs of 58S scaffolds foamed using different amounts of surfactant. Fig. 2a shows a foam made with 1 ml Teepol. The scaffold exhibited a bulk density (ρ_b) of 0.60 gcm^{-3} from a foam volume of 65 ml, which was only slightly lower than the ρ_b of a 58S monolith (0.86 gcm^{-3}), implying that the total macropore volume was low. Fig. 2a shows that

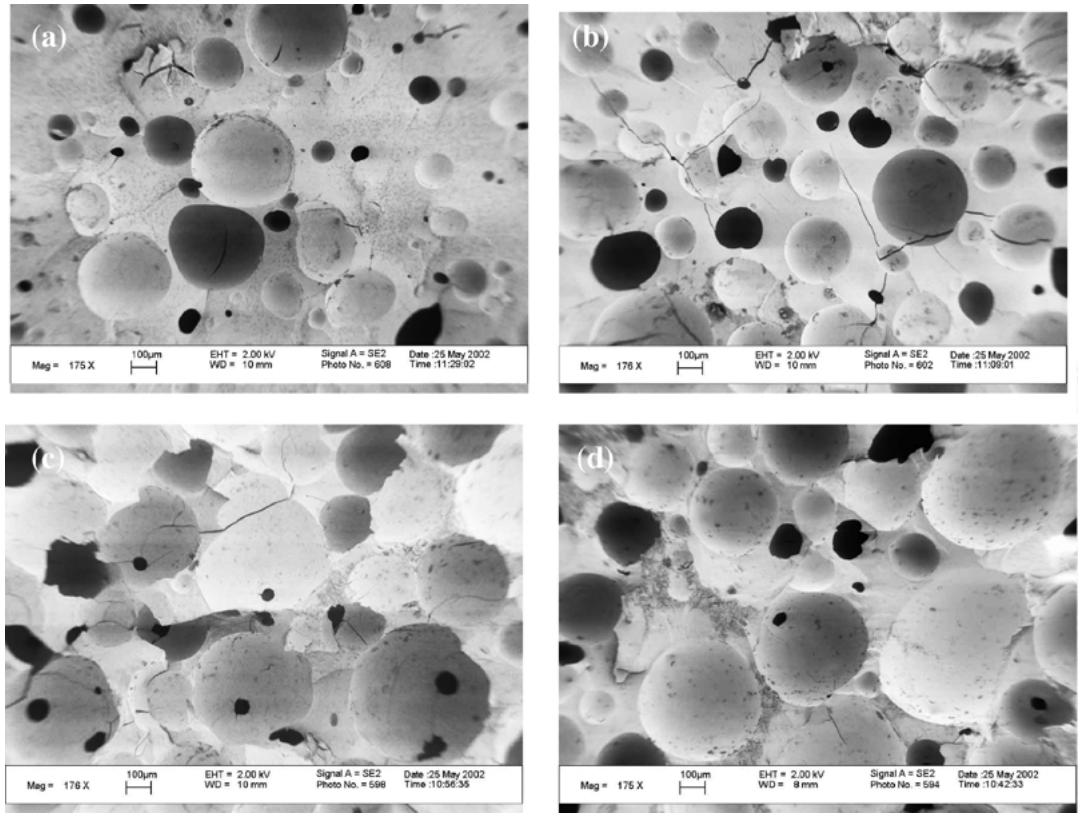

Figure 2 SEM micrographs of 58S scaffolds foamed with (a) 1 ml Teepol ($\rho_b = 0.50$ gcm^{-3}), (b) 1.5 ml Teepol ($\rho_b = 0.39$ gcm^{-3}), (c) 2 ml Teepol ($\rho_b = 0.35$ gcm^{-3}), and (d) 3 ml Teepol ($\rho_b = 0.41$ gcm^{-3}).

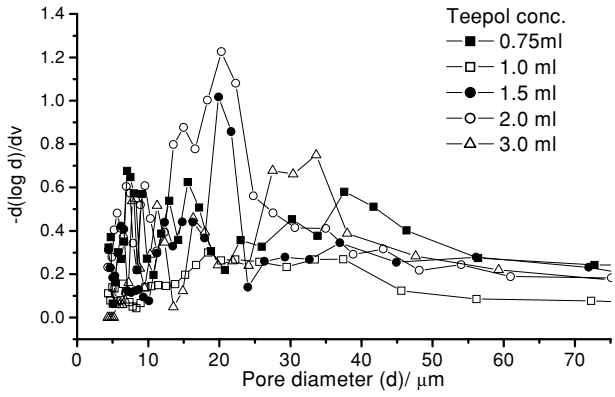

Figure 3 Interconnected macropore size distribution for 58S foams as function of surfactant concentration, obtained from mercury intrusion porosimetry.

although there were some spherical pores in excess of 200 μm in diameter, the pore walls were very thick, and there were no windows leading to other pores. The foam had a closed cell structure with isolated pores and the structure was cracked. The foam was very fragile and difficult to handle.

Fig. 2c shows that as surfactant concentration increased to 2 ml (foam volume of 106 ml), and ρ_b decreased to 0.35 gcm^{-3}, the number of macropores increased further and the mean pore diameter also increased, causing the majority of pores to share pore edges and interconnectivity to increase. Many pore walls contained pore windows of up to 80 μm in diameter, creating an open cell structure. As surfactant concentration increased from 2 ml to 3 ml, there was no apparent increase in macropore size or interconnectivity. This is because the mean foam volume did not increase above 104 ml as surfactant concentration increased. Cracks were still present but were fewer in number compared to the scaffolds with higher ρ_b values, therefore handling strength of the 58S foams seemed to increase as bulk density decreased.

Fig. 3 shows the interconnected macropore distribution determined from mercury intrusion porosimetry for 58S foams of different surfactant concentrations. The vertical axis ($-\mathrm{d}V/d\log D$) is a differential of the volume of mercury intruded (V) at each interconnected pore diameter (D). For tissue engineering applications, the modal interconnected pore diameter is the most important parameter of the pore network, as it indicates the largest number of pores of that diameter in the pore network. Fig. 3 shows that the modal interconnected pore diameter increased from 7 μm at 0.75 ml Teepol to approximately 20 μm and 34 μm at 2 ml and 3 ml Teepol respectively. In order to produce 58S foams with modal interconnected pore diameters in excess of 100 μm, water must be added to aid the surfactant at the foaming stage [7].

3.2.2. 70S30C foam

Fig. 4 shows SEM micrographs of 70S30C scaffolds foamed using (a) 0.5 ml Teepol ($\rho_b = 0.25$ gcm^{-3}), (b) 0.65 ml Teepol ($\rho_b = 0.18$ gcm^{-3}), (c) 0.75 ml Teepol ($\rho_b = 0.15$ gcm^{-3}), and (d) 1 ml Teepol ($\rho_b = 0.15$ gcm^{-3}). The amount of surfactant used was lower than for 58S, due to 70S30C being more susceptible to foaming (Fig. 1). Table I shows that this greater susceptibility to foaming produced scaffolds with lower

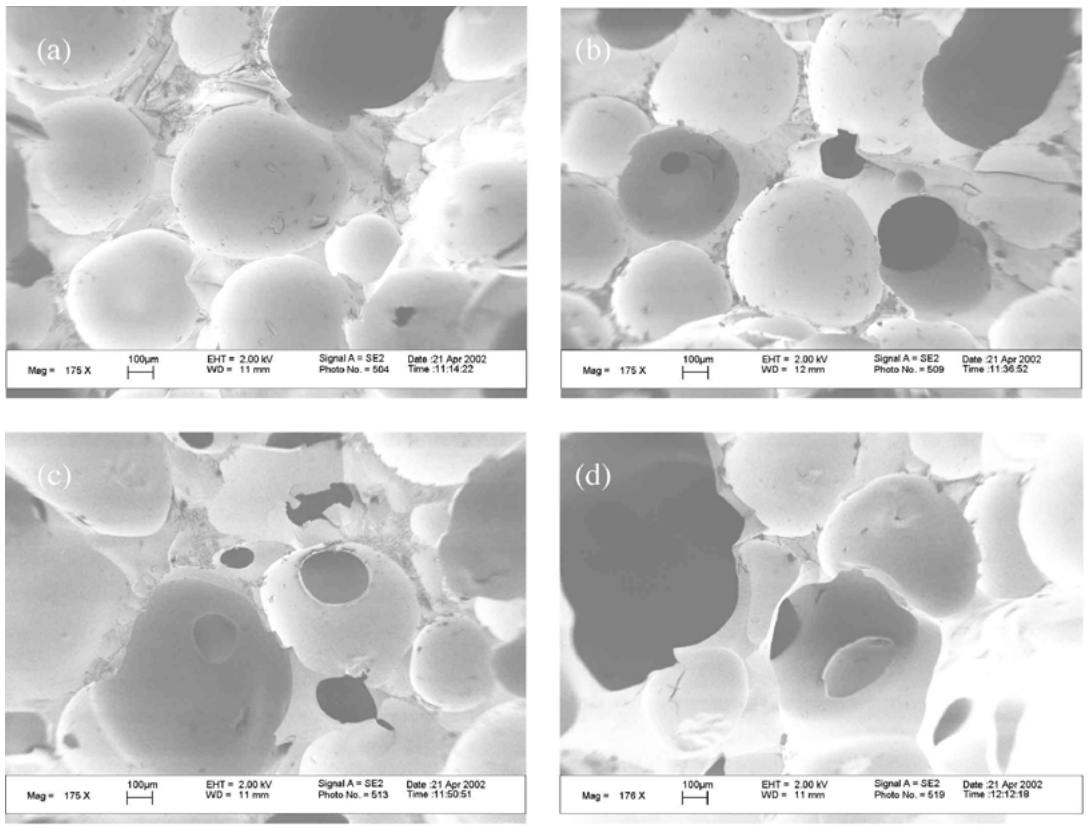

Figure 4 SEM micrographs of 70S30C foam scaffolds prepared with (a) 0.5 ml Teepol ($\rho_b = 0.25$ gcm^{-3}), (b) 0.65 ml Teepol ($\rho_b = 0.18$ gcm^{-3}), (c) 0.75 ml Teepol ($\rho_b = 0.15$ gcm^{-3}), and (d) 1 ml Teepol ($\rho_b = 0.15$ gcm^{-3}).

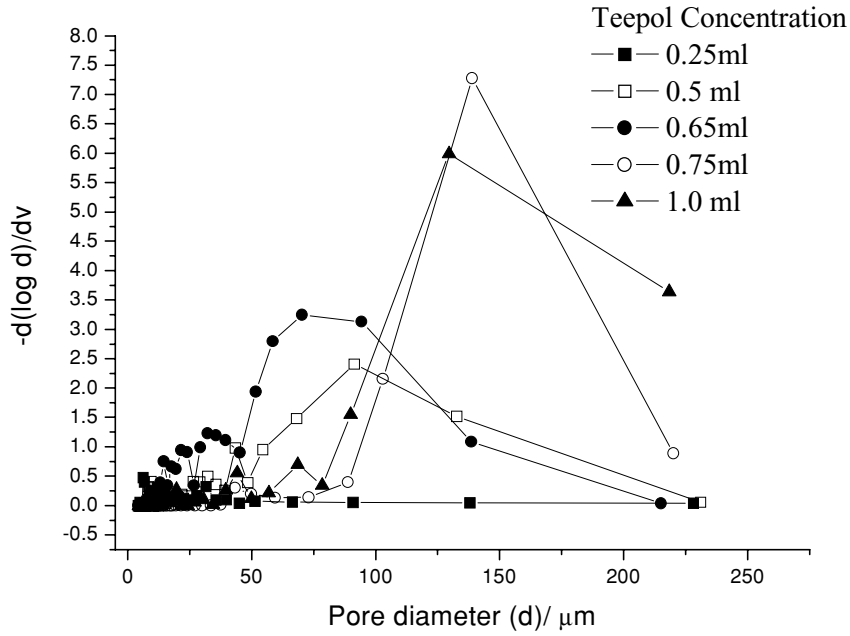

Figure 5 Interconnected macropore size distribution for 70S30C foams as function of surfactant concentration, obtained from mercury intrusion porosimetry.

ρ_b. The minimum ρ_b achieved for 58S foams was 0.35 gcm^{-3} (at 2 ml Teepol) compared to 0.15 gcm^{-3} (at 1 ml Teepol) for 70S30C. The lower bulk density of 70S30C foams resulted in larger pores, thinner cell walls, greater homogeneity and a generally more open cell structure than the 58S foams. Fig. 4a shows that using just 0.5 ml Teepol produces a highly porous crack free scaffold with some degree of interconnectivity. Fig. 4c shows that using 0.75 ml Teepol produced a scaffold with a very homogenous and highly interconnected porous structure. Fig. 4d shows that as surfactant concentration was increased to 1 ml Teepol the pore network became less homogeneous, but many of the pores were opened up into interconnected channels with diameters up to 400 μm.

Fig. 5 shows the interconnected macropore size distribution for 70S30C foams as function of surfactant concentration, obtained from mercury intrusion porosimetry. Fig. 5 shows that as the surfactant concentration increased, the modal interconnected pore diameter (d_{mod}) generally increased. The d_{mod} was approximately the same at 0.5 ml Teepol and 0.65 ml Teepol. However, as Teepol concentration increased to 0.75 ml, large increases in d_{mod} and in the number of pores were observed. As the surfactant concentration increased to 1 ml, d_{mod} did not increase, but the pore size distribution was wider, implying more pores were present at higher pore diameters. A limitiation to this technique is that the porosimeter could not detect pores greater than 250 μm in diameter. Scaffolds foamed with 0.75 ml surfactant exhibited a bulk density of 0.15 gcm^{-3} and a modal interconnected pore diameter of $\sim$140 μm, whereas a scaffold foamed with 0.25 ml surfactant exhibited a bulk density of 0.33 gcm^{-3} and a modal interconnected pore diameter of just 6 μm. Fig. 5 shows that small differences in surfactant concentration can have a large effect on the interconnected pore network; a scaffold foamed with 0.65 ml surfactant exhibited a bulk density of 0.18 gcm^{-3}, only 0.03 gcm^{-3} higher than the scaffolds foamed with 0.75 ml surfactant. However, the former exhibited a modal interconnected pore diameter of 86 μm, 60% of that of the latter.

3.2.3. 100S foams

The 100S pure silica foams shown in Fig. 6 exhibited a similar relationship between surfactant concentration and pore size to the 58S and 70S30C foams. However, the foams were structurally weak, due to cracks initiating during the drying and stabilisation stages of the foaming process. Pore sizes were generally lower than in the 70S30C foams, but appeared to be larger and more interconnected than the 58S foams with macropores in excess of 500 μm and pore windows in excess of 100 μm in diameter. The 100S scaffolds had a very low handling strength and were too fragile for mechanical testing. Minimum ρ_b was 0.16 gcm^{-3} at a Teepol concentration of 3 ml compared with 0.75 gcm^{-3} at 0.75 ml Teepol for 70S30C and 0.34 gcm^{-3} at 2 ml Teepol for 58S. At a Teepol concentration of 0.75 ml, the modal interconnected pore diameter (d_{mod}) was 44 μm but increased to between 50 and 71 μm for Teepol concentrations between 1 and 3 ml, which was approximately double the maximum d_{mod} value for 58S and just over half that for 70S30C, which correlates with the foam volumes produced (Fig. 1).

3.3. Mesoporous texture

Fig. 7 shows the textural pore size distribution of 58S scaffolds, foamed at different surfactant concentrations, obtained by the BJH method from nitrogen sorption isotherms. Fig. 7 shows that the textural porosity was within the mesoporous range (2–50 nm). Similar

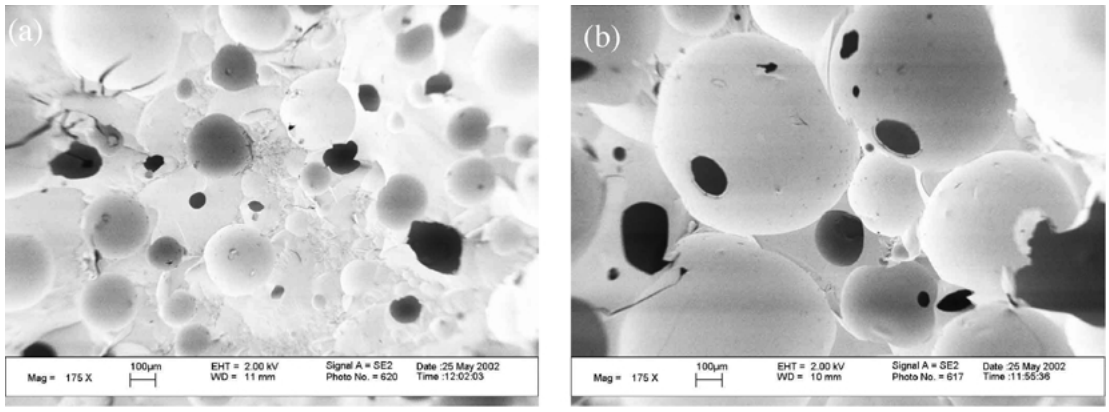

Figure 6 SEM micrographs of 100S scaffolds foamed with (a) 0.5 ml Teepol ($\rho_b = 0.27$ cm^{-3}), (b) 1 ml Teepol ($\rho_b = 0.24$ gcm^{-3}).

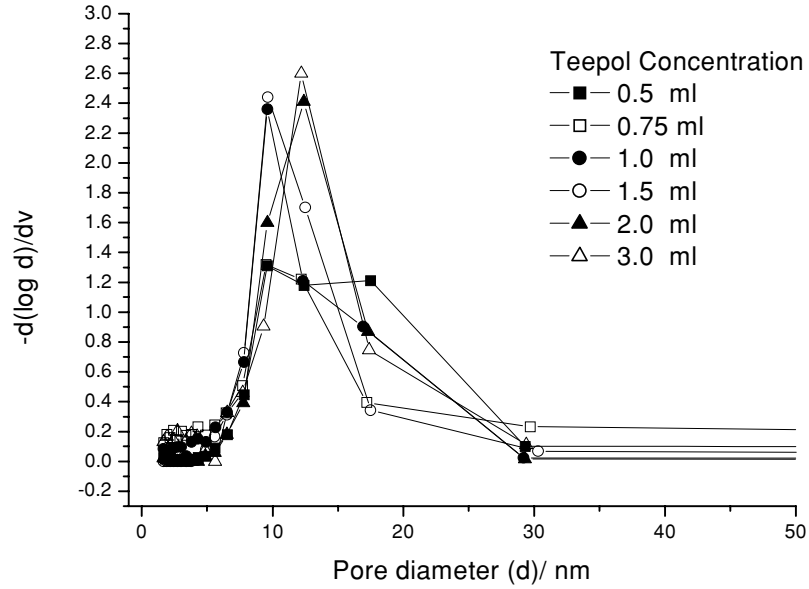

Figure 7 Textural pore size distribution of 70S30C foams as a function surfactant concentration, obtained by the BJH method from nitrogen sorption isotherms.

distributions are exhibited by the 100S and 70S30C compositions (not shown). The modal mesopore diameters are listed in Table I for each glass composition. Values did not seem to change greatly as surfactant concentration increased, for each composition. Modal mesopore diameters for 70S30C and 100S were almost double (both approximately 17 nm) that for the 58S glasses (approximately 9 nm).

3.4. Unfoamed monoliths

The BJH pore size distributions (not shown) were also obtained from nitrogen sorption analysis on monoliths that were prepared in the manner as the foams except they were not agitated. Changing the surfactant concentration did not affect the modal textural pore diameter (Table I); it was always approximately 12 nm. 58S monoliths all exhibited modal pore diameters of approximately 12 nm for all surfactant concentrations.

4. Discussion

Fig. 1 showed that the 70S30C system was more susceptible to the foaming process than the 58S and 100S compositions. The marked difference in foamability between the binary 70S30C system over the 100S system (Fig. 1) is thought to be due to the presence of CaO as network modifier. For each composition, the majority of foam formation occurred as the viscosity of the sol started to increase substantially, i.e., approximately 4 min after HF addition (the lag time). The increase in viscosity corresponds to the formation of the gel structure, i.e., the formation of the silica network by the polycondensation reaction [16]. Although the final glass structure is determined after gelation, it originates during gelation and the composition of the sol may affect the way the network forms and therefore how the viscous sol foams.

The network structure of 100S gel-glass consists primarily of silica tetrahedra, i.e. silicon atoms bonded by 4 bridging oxygen bonds (O─Si─O) called a Q_4 structure [17]. The addition of CaO to the system may create silica tetrahedra with non-bridging oxygen ions (NBOs). As CaO content increases the Q_4 structure would become a Q_3 structure (3 bridging oxygens). As CaO content increases to 50 mol% CaO a Q_2 structure would be formed. At a composition of 36 mol% CaO there should be 1 to 2 NBOs per silica tetrahedra, forming a more open network than the 100S.

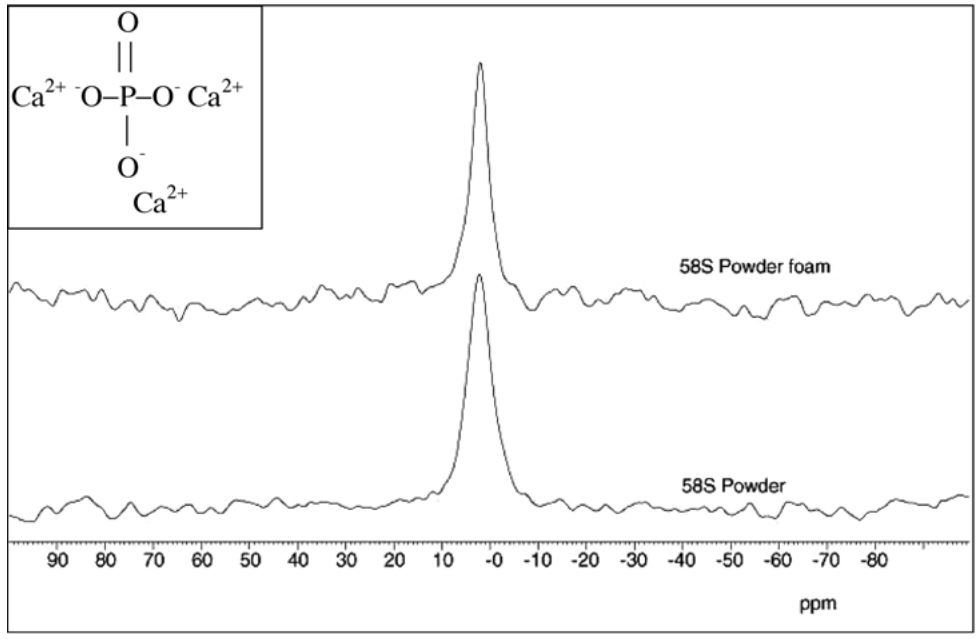

Figure 8 ^{31}P MAS-NMR spectrum of 58S foam (courtesy of Dr. A. Stamboulis) and the calcium orthophosphate structure (insert).

The network would be a mixture of Q_3 and Q_2 structural units.

Fig. 8 shows a ^{31}P MAS-NMR (magic angle scattering nuclear magnetic resonance) spectrum for a 58S foam produced with 1.5 ml surfactant and a powder produced using the standard sol-gel procedure, i.e., without agitation or the addition of HF or Teepol [9]. Fig. 8 shows that 58S gel-glass powders and foams contain orthophosphate structures, i.e., addition of phosphate brings some of the network modifying Ca^{2+} ions into the network, forming $Ca_3(PO_4)_2$ [18]. Fielder [19] also found orthophosphate in 58S gel-derived monoliths. The orthophosphate structure is shown in the insert of Fig. 8.

Calcium ions that would have formed NBOs may have been taken into the network to form $Ca_3(PO_4)_2$, causing the structure of the 58S gel-glass to tend towards a Q_3 structure, rather than Q_2, increasing the network connectivity of the glass and reducing the foamability. This theory assumes that OH^- content of 100S, 70S30C and 58S sols were constant because OH^- causes formation of Si–OH groups in the network, also reducing network connectivity. All sols were prepared with excess water (high water/TEOS ratio) for the hydrolysis of the TEOS, which should reduce the number of silanol groups formed during the initial formation of the silica network.

Another contributing factor, to the difference in foamability for the 3 glass compositions, could be that the water/TEOS (R) ratio was higher for 100S and 70S30C ($R = 12$) than for 58S ($R = 8$). This higher water concentration may not only aid surfactant activity, but also cause the glass network to have a greater initial pore diameter and surface area, providing more sites for surfactant interaction [20].

For each composition, above a certain surfactant concentration the foam volume did not increase as surfactant concentration increased; above a critical concentration of surfactant the solution becomes saturated with surfactant. Surfactants are amphiphilic macromolecules that are composed of two parts, one hydrophobic and one hydrophilic [21]. Owing to this configuration, surfactants tend to adsorb onto gas-liquid interfaces with the hydrophobic part being expelled from the solvent and a hydrophilic part remaining in contact with the liquid. This behaviour lowers the surface tension of the gas-liquid interfaces, making the foam films thermodynamically stable, which would otherwise collapse in the absence of surfactant. On saturation there are no longer any water molecules to bond to the hydrophilic part of surfactant. Rings of surfactant molecules (micelles) are formed and the CMC (critical micelle concentration) is reached [21]. Addition of more surfactant does not increase bubble film stability any further, but instead is a detriment to strength of the silica network [22]. The superior foamability of the 70S30C system accounts for the lower concentrations of surfactant required to saturate the solution.

Without the addition of water at the foaming stage, the maximum modal interconnected pore diameter in 58S foams was 38 μm, compared to >100 μm achieved in previous work. An advantage of the 70S30C system is that the extra water addition is not required to attain large interconnected pores (Fig. 4).

In addition to being more susceptible to the foaming process the 70S30C foams exhibited much greater handling strength than both 58S and 100S foams. The critical stage of the foaming process for the production of crack-free foam scaffolds is the drying stage of the sol-gel process. During the drying stage, liquid (water and alcohol) produced by the polycondensation reaction is evaporated from within the pore network. Therefore narrow interconnected pore channels, such as those exhibited by the 58S and 100S foams, cause build up of high capillary stresses, which cause cracks to nucleate at the pore edges.

5. Conclusions

The three glass compositions (58S, 70S30C and 100S) were successfully foamed to produce stable porous scaffolds with potential for tissue engineering scaffolds. Pore networks with different characteristics were produced. The pore network properties can be controlled by the surfactant concentration used in the foaming process. As foam volume increased, and bulk density decreased, interconnections between macropores were larger, more frequent and more regular in shape.

The 70S30C system was the most susceptible to foaming and the 58S system the least susceptible to foaming. In each system, the foam volume attained, from 50 ml sol, increased as surfactant concentration increased, up until a critical surfactant concentration, where the solution saturated and micelles were formed.

As foam volume increased, interconnected pore size also increased in each system. Therefore, the 70S30C system exhibited the greatest maximum modal interconnected pore diameter (140 μm, compared to the 34 μm of the 58S system). The mesoporous texture of the gel-glasses was unaffected by the addition of surfactant and the foaming process.

Acknowledgements

The work was funded by the EPSRC and Lloyd's Tercentary Foundation. The authors would like to thank Dr. Artemis Stamboulis and Mr. Nick Royall for NMR and SEM assistance respectively.

References

1. R. LANGER and J. P. VACANTI, *Science* **260**(5110) (1993) 920.
2. J. R. JONES and L. L. HENCH, *J. Mat. Sci. T.* **17** (2001) 891.
3. H. OONISHI, L. L. HENCH, J. WILSON, F. SUGIHARA, E. TSUJI, M. MATSURA, S. KIN, T. YAMAMOTO and S. MIZOKAWA, *J. Biomed. Mater. Res.* **51** (2000) 37.
4. L. L. HENCH, *J. Amer. Ceram. Soc.* **74**(7) (1991) 1487.
5. I. D. XYNOS, A. J. EDGAR, L. D. K. BUTTERY, L. L. HENCH and J. M. POLAK, *Bioc. Biop. R.* **276**(2) (2000) 461.
6. T. M. FREYMAN, I. V. YANNAS and L. J. GIBSON, *Prog. Mater. Sci.* **46** (2001) 273.
7. P. SEPULVEDA, J. R. JONES and L. L. HENCH *J. Biomed. Mater. Res.* **59**(2) (2002) 340.
8. *Idem.*, *ibid.* **61**(2) (2002) 301.
9. R. LI, A. E. CLARK and L. L. HENCH, *ibid.* **2** (1991) 231.
10. D. C. GREENSPAN, J. P. ZHONG, Z. F. CHEN and G. P. LATORRE, in Proceedings of 10th International Symposium on Ceramics in Medicine, Bioceramics; 10, edited by L. Sedel and C. Rey (Pergamon Press, Oxford, 1997) p. 391.
11. M. M. PEREIRA and L. L. HENCH, *J. Sol-Gel S.* **7** (1996) 59.
12. P. SARAVANAPAVAN and L. L. HENCH, *J. Biomed. Mater. Res.* **54**(4) (2001) 608.
13. C. LEON, *Adv. Coll In.* **77** (1998) 341.
14. N. J. COLEMAN and L. L. HENCH, *Cer. Int.* **26** (2000) 171.
15. P. SEPULVEDA and J. G. P. BINNER, *J. Eur. Ceram. Soc.* **19**(12) (1999) 2059.
16. L. L. HENCH and J. K. WEST, *Chem. Rev.* **90** (1990) 33.
17. H. DOWEIDAR, *Phys. C. Glas.* **40**(2) (1999) 85.
18. M. W. G. LOCKYER, D. HOLLAND and R. DUPREE, *J. Non-Cryst. Sol.* **188** (1995) 207.
19. E. FIELDER, PhD Thesis, Imperial College London, 2002.
20. L. C. KLEIN and G. J. GARVEY, in "Ultrastructure Processing of Ceramics, Glasses and Composites" edited by L. L. Hench and D. R. Ulrich (John Wiley and Sons, New York, 1984) p. 88.
21. M. J. ROSEN, "Surfactants and Interfacial Phenomena," 2nd ed. (John Wiley & Sons, New York, 1989).
22. F. S. ORTEGA, P. SEPULVEDA, M. D. M. INNOCENTINI and V. C. PANDOLFELLI, *Amer. Ceram. Soc.* **80**(4) (2001) 37.

Received 11 November 2002
and accepted 7 July 2003